COMPARISON OF CURRENT VECTOR CONTROL AND FLUX VECTOR CONTROL STRATEGIES FOR PERMANENT MAGNET SYNCHRONOUS MOTOR DRIVES

Ton That Dong[1*], Nguyen Khanh Quang[2], Nguyen Dang Khoa[3]

[1]*Hue Industrial College*

[2]*University of Science and Technology - The University of Danang*

[3]*SYSBOTIX Solution Join Stock Company*

*Email: *ttdong@hueic.edu.vn*

Received: 6 May 2024; Accepted: 31 May 2024

ABSTRACT

This study compares the effectiveness of Current Vector Control (CVC) and Flux Vector Control (FVC) methods for Surface-mounted Permanent Magnet Synchronous Motor (SPMSM) drives. The control strategies of both methods are analyzed and represented in this work. Through simulation, the dynamic performance of the motor produced by both methods is evaluated and compared in terms of both transient- and steady-state behaviors. The insights gained from this analysis assist engineers in selecting the most suitable control strategy for PMSM applications.

Keywords: Current vector control, Flux vector control, PMSM, Field-oriented control.

1. INTRODUCTION

Recently, eco-friendly industrial strategies have been widely adopted to mitigate global greenhouse gas emissions. Consequently, there is a growing demand for high-performance electric drives and power plants. The Permanent Magnet Synchronous Motor (PMSM) plays a crucial role in this trend due to its remarkable advantages, including a wide speed range at constant power, high efficiency, high power and torque density, and low maintenance cost. The PMSM features an approximately sinusoidal back electromotive force (B-EMF) and air-gap flux distribution, resulting from the three-phase sinusoidal current distributed in the stator windings. This sets it apart from Brushless DC Motors (BLDC), which are powered by square current distribution and exhibit trapezoidal distribution of B-EMF and air-gap flux. As a result, the PMSM delivers smoother torque and lower harmonic current compared to BLDC, requires less maintenance, and is safer for use in explosive environments than DC motors [1, 2]. Unlike Induction Motors (IM), PMSM does not require excitation currents in the rotor and contains less iron, leading to increased efficiency and reduced costs compared to IMs. Due to these numerous advantages, the PMSM has gained traction in both industrial and household applications [1, 2].

Moreover, the demand for a highly efficient PMSM drive with superior dynamic performance, accuracy, robustness, and simplicity is paramount, given its wide range of applications. Current and flux linkage vectors are recognized as crucial state variables as they accurately depict the operating conditions of a PMSM across various scenarios. Consequently, they serve as primary components in numerous vector control methods for PMSM drives [3-8], including Current Vector Control (CVC) and Flux Vector Control (FVC).

This study delves into the analysis of current and flux linkage vectors to elucidate their fundamental principles in control structure. It aims to highlight the respective advantages and disadvantages of these vectors, thereby offering valuable insights into their applicability. Finally, the efficacy and reliability of both control methods are comprehensively assessed and validated through simulations conducted on a surface-mounted Permanent Magnet Synchronous Motor drive (SPMSM).

2. PRINCIPLE OF PMSM MATHEMACTICAL MODELING, CURRENT VECTOR CONTROL AND FLUX VECTOR CONTROL

2.1. PMSM mathematical model in the rotor PM flux coordinate ($d-q$)

The general voltage vector equation is written as

$$\vec{v}_s = R_s\vec{i}_s + \frac{d\vec{\Psi}_s}{dt} \tag{1}$$

where $\vec{v}_s, \vec{i}_s,$ and $\vec{\Psi}_s$ are stator voltage, current and flux linkage vectors, respectively and R_s is the winding resistance.

The voltage equation in the rotor rotating frame can be shown as

$$\begin{bmatrix} v_d \\ v_q \end{bmatrix} = R_s \begin{bmatrix} i_d \\ i_q \end{bmatrix} + \frac{d}{dt}\begin{bmatrix} \Psi_d \\ \Psi_q \end{bmatrix} + \omega_e \begin{bmatrix} -\Psi_q \\ \Psi_d \end{bmatrix} \tag{2}$$

where $\begin{bmatrix} v_d \\ v_q \end{bmatrix}$, $\begin{bmatrix} i_d \\ i_q \end{bmatrix}$ and $\begin{bmatrix} \Psi_d \\ \Psi_q \end{bmatrix}$ are the matrices of projection components on $d-q$ frame of stator voltage, current and flux linkage vectors, respectively and ω_e is the electrical angular speed.

The *dq*-axis flux linkage formulae are calculated as

$$\begin{cases} \Psi_d = \Psi_m + L_d i_d \\ \Psi_q = L_q i_q \end{cases} \tag{3}$$

$$\Psi_s = \sqrt{\Psi_d^2 + \Psi_q^2} \tag{4}$$

where Ψ_m is PM flux linkage in *d*-axis, L_d and L_q are stator inductances on $d-$ and $q-$axis, respestively.

Substituting (3) into (2), the *dq*-axis voltage equation yields

$$\begin{bmatrix} v_d \\ v_q \end{bmatrix} = \begin{bmatrix} R_s & -\omega_e L_q \\ \omega_e L_d & R_s \end{bmatrix}\begin{bmatrix} i_d \\ i_q \end{bmatrix} + \begin{bmatrix} L_d & 0 \\ 0 & L_q \end{bmatrix}\frac{d}{dt}\begin{bmatrix} i_d \\ i_q \end{bmatrix} + \omega_e \begin{bmatrix} 0 \\ \Psi_m \end{bmatrix} \tag{5}$$

If $L_d = L_q = L_s$ in SPMSM, then (5) turns into

$$\begin{bmatrix} v_d \\ v_q \end{bmatrix} = \begin{bmatrix} R_s & -\omega_e L_s \\ \omega_e L_s & R_s \end{bmatrix}\begin{bmatrix} i_d \\ i_q \end{bmatrix} + L_s\frac{d}{dt}\begin{bmatrix} i_d \\ i_q \end{bmatrix} + \omega_e \begin{bmatrix} 0 \\ \Psi_m \end{bmatrix} \tag{6}$$

where L_s is the stator inductance of SPMSM in the rotor flux coordinate.

The electromagnetic torque can be rewritten as

$$T_e = \frac{3}{2}p_n\left|\vec{\Psi}_s \times \vec{i}_s\right| \tag{7}$$

$$\therefore T_e = \frac{3}{2}p_n\left[\Psi_m i_q + \left(L_d - L_q\right)i_d i_q\right] \tag{8}$$

where T_e is the electromagnetic torque and p_n is the number of pole-pairs.

Note that in case of SPMSM, $L_d = L_q$, the equation (8) is rewritten as

$$T_e = \frac{3}{2} p_n \Psi_m i_q \tag{9}$$

On the other hand, the electromagnetic torque can be rewritten toward the relationship of stator flux linkage and PM flux linkage vectors and formula given as

$$T_e = \frac{3}{2} p_n \frac{\Psi_m \Psi_s \sin\delta}{L_s} \tag{10}$$

$$\therefore T_e = \frac{3}{2} p_n \frac{\left|\vec{\Psi}_m \times \vec{\Psi}_s\right|}{L_s} \tag{11}$$

where δ is the load angle defined by the angle between the stator and PM flux linkage vectors.

As seen in (11), the electromagnetic torque in SPMSM is the result of the vector product of PM flux and stator flux linkage.

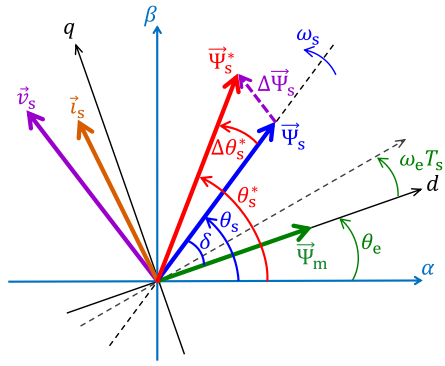

Figure 1. Phasor diagram of PMSM model

2.2. Curent Vector Control method

The CVC or Field-Oriented Control (FOC) [3, 4] is an advanced high-performance control scheme introduced in 1970 and adopted popularly in industrial AC drive systems until now.

The principle of FOC method is altering the AC motor traditional control method from scalar control to vector control via analyzing the current vector in a rotating coordinate oriented over the rotor flux linkage vector. That is the reason why FOC needs a synchronously rotating reference frame with rotor and the rotor position information is mandatory. As a result, AC motor control has been like DC motor control, with the torque and flux linkage are decoupled to control via the two orthogonal elements in the $d-q$ frame of the current vector. The rotor flux linkage is produced in the *d*-axis by the permanent magnet while the stator flux linkage is generated in both the *d* and *q*-axis via the CVC by regulating the current vector. To achieve maximum torque per ampere (MTPA) for SPMSM, the current vector should align with the *q*-axis since torque is linearly proportional to the *q*-axis current component, as shown in equation (9). Therefore, two PI controllers are employed to regulate the *d*- and *q*-axis current components in the CVC scheme. As a result, the output currents can be simply limited and precisely controlled.

Based on (6), the block diagram of the CVC with speed control mode for SPMSM drive is built as shown in Fig. 2.

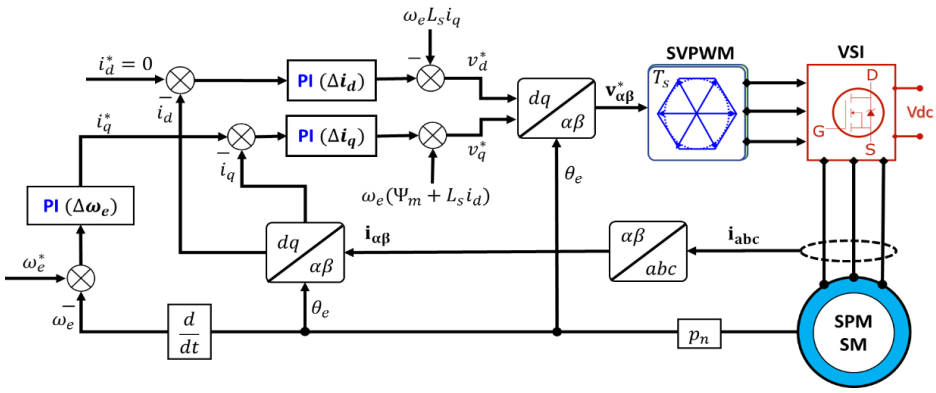

Figure 2. Block diagram of the CVC scheme

2.3. Flux Vector Control method

In the FVC scheme [5-8], the voltage vector command is determined based on the deviation of the reference and estimated stator flux linkage vectors within each control period, which is called a reference flux vector calculation expression. Accordingly, only one used PI controller of torque computes the load angle increment to control the phase angle of the flux linkage vector, and the calculations are directly performed in stationary coordinates.

From general voltage vector equation (1) in the time-domain is discretized by the sampling time T_s [6] into

$$\vec{v}_s(k+1) = R_s\vec{i}_s(k) + \frac{\vec{\Psi}_s(k+1) - \vec{\Psi}_s(k)}{T_s} \tag{12}$$

$$\therefore \vec{v}_s^* = R_s\vec{i}_s + \frac{\vec{\Psi}_s^* - \vec{\Psi}_s}{T_s} = R_s\vec{i}_s + \frac{\Delta\vec{\Psi}_s}{T_s} \tag{13}$$

where (k) or $(k+1)$ indicates the kth or $(k+1)$th sampling period, the symbol $\square^*$ (upper star) is used to denote a desired or reference value, T_s is the control loop sample time and $\Delta\vec{\Psi}_s$ is the displacement vector between actual and reference flux linkage vectors.

Hence, by (13), the vectors can be rewritten in $(\alpha - \beta)$ coordinate as

$$\begin{bmatrix} v_\alpha^* \\ v_\beta^* \end{bmatrix} = R_s \begin{bmatrix} i_\alpha \\ i_\beta \end{bmatrix} + \frac{1}{T_s}\left(\begin{bmatrix} \Psi_\alpha^* \\ \Psi_\beta^* \end{bmatrix} - \begin{bmatrix} \hat{\Psi}_\alpha \\ \hat{\Psi}_\beta \end{bmatrix} \right) \tag{14}$$

where the symbol $\hat{\square}$ (hat) is used to denote an estimated value, $\begin{bmatrix} v_\alpha \\ v_\beta \end{bmatrix}$, $\begin{bmatrix} i_\alpha \\ i_\beta \end{bmatrix}$ and $\begin{bmatrix} \Psi_\alpha \\ \Psi_\beta \end{bmatrix}$ are the stator voltage, current and flux linkage in $\alpha - \beta$ frame, respectively.

The flux linkage reference $\begin{bmatrix} \Psi_\alpha^* \\ \Psi_\beta^* \end{bmatrix}$ is determined by amplitude and phase angle of flux linkage vector reference $\vec{\Psi}_s^*$ as

$$\begin{bmatrix} \Psi_\alpha^* \\ \Psi_\beta^* \end{bmatrix} = \begin{bmatrix} \Psi_s^* \cos(\theta_s^*) \\ \Psi_s^* \sin(\theta_s^*) \end{bmatrix} \tag{15}$$

where θ_s^* is the phase angle of flux linkage vector reference.

The magnitude of flux linkage vector reference Ψ_s^* in (15) is calculated from torque reference T_e^* by MTPA optimum method as

$$\Psi_s^* = \sqrt{\Psi_m^2 - \left(\frac{L_s}{\frac{3}{2}p_n\Psi_m}T_e^*\right)^2} \tag{16}$$

According to (10), it can be concluded that if assuming flux linkage magnitude is constant in steady state, the torque produced will be significantly decided by the controlled load angle δ. It means that the error of torque (between reference and current values) can be reduced by controlling load angle deviation $\Delta\delta$ during operation. Therefore, the load angle deviation command $\Delta\delta^*$ is generated by a torque regulator, which utilizes a PI controller to minimize torque error.

As seen in Fig. 1, the phase angle of flux linkage vector reference (θ_s^*) can be defined based on $\Delta\delta^*$, the current position of the flux linkage vector and the incremental angle respective to the rotor movement over time [6]. The formula is expressed as

$$\theta_s^* = \hat{\theta}_s + \Delta\delta^* + \omega_e T_s \tag{17}$$

Ultimately, the block diagram of the FVC is presented in Fig. 3.

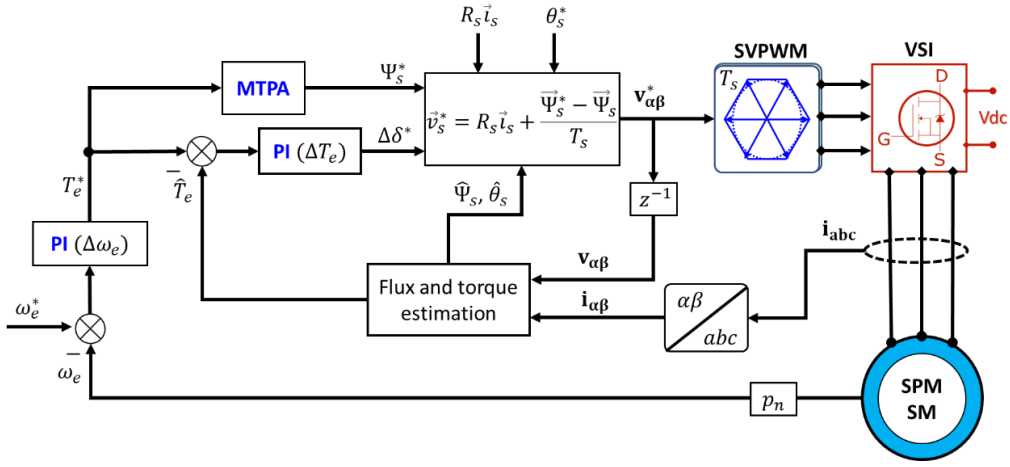

Figure 3. Block diagram of the FVC scheme for SPMSM drive

It becomes apparent that the FVC scheme in Fig. 3 offers a simpler configuration compared to the CVC scheme depicted in Fig. 2. This simplicity arises from the absence of frame transformation and the utilization of only one PI controller for torque regulation, resulting in reduced computational complexity and parameter dependence compared to the CVC scheme. However, it's worth noting that in the FVC scheme, estimation techniques are required to determine flux linkage and torque values [6, 9], adding a layer of complexity to the control process.

2.4. Space vector pulse width modulation (SVPWM)

The SVPWM [8] is used to approximately convert a reference voltage vector, $\vec{V}_{ref}$, directly into switch turning duties for a voltage source inverter (VSI). With the 2-level of a 3-phase VSI, it has eight inverter switching status based on the status of the upper switches, they generate eight terminal voltages in three phases of motor and converted to eight voltage vectors including six active (non-zero) vectors ($\vec{V}_1 - \vec{V}_6$) and two zero (null) vectors ($\vec{V}_0$ and $\vec{V}_7$). Principally, they can be mapped into the vertices of a regular hexagon in the stationary frame and created the six sub triangles (named Sector 1, …, Sector 6) as shown in Fig. 4.

The eight voltage vectors formed by the upper switch states are presented as follows

$$\vec{V}_k = \frac{2}{3} V_{dc}(S_a + \boldsymbol{a} S_b + \boldsymbol{a}^2 S_c) \text{ with } \boldsymbol{a} = e^{\frac{j2\pi}{3}}, k = 0..7 \quad (18)$$

where $\vec{V}_k$ is the kth voltage vector and V_{dc} is the DC voltage of source. The vectors, $\vec{V}_1..\vec{V}_6$, are called the active vector, while the vectors, V_0 and V_7, are called the zero-voltage vectors.

An arbitrary reference voltage vector can be represented by the following formula

$$\vec{V}_{ref} = \frac{T_L}{T_c}\vec{V}_{L,m} + \frac{T_R}{T_c}\vec{V}_{R,m} + 2\frac{T_0}{T_c}\vec{V}_z \quad (19)$$

$$\therefore \vec{V}_{ref} = \vec{V}_L + \vec{V}_R \quad (20)$$

$$T_c = T_L + T_R + 2T_0 \quad (21)$$

where $\vec{V}_{ref}$ is the reference voltage vector modulated, $\vec{V}_{L,m}$ and $\vec{V}_{R,m}$ are the left and right active voltage vectors in sector m, respectively, $\vec{V}_z$ is the zero-voltage vector, T_L, T_R and T_0 are the on-duty times under a switching period (T_c) of the vectors $\vec{V}_{L,m}, \vec{V}_{R,m}$ and $\vec{V}_z$, respectively, $\vec{V}_L$ and $\vec{V}_R$ are the left and right equivalent voltage vectors determined by activating $\vec{V}_{L,m}, \vec{V}_{R,m}$ and $\vec{V}_z$ over corresponding the on-duty times, T_L, T_R and T_0.

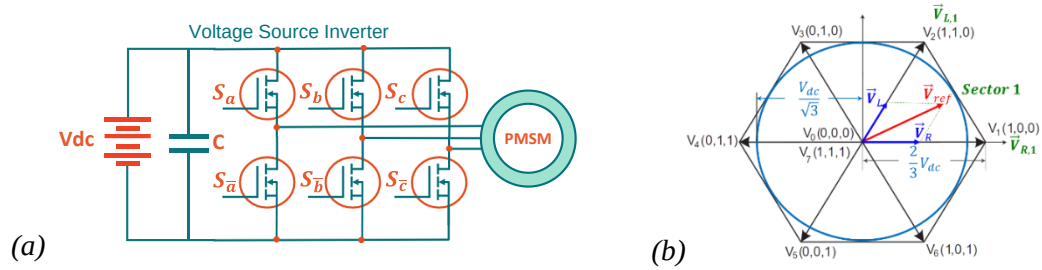

Figure 4. (a) The circuit diagram of a voltage source inverter 3-phase 2-level and *(b)* Voltage space vector hexagon

For example, a case of the modulated $\vec{V}_{ref}$ when lying under Sector 1 is represented in Fig. 4(b). As seen in Fig. 4(b) that at any given time, a reference voltage vector will inhabit a certain sector. Then it is approximated by a vector sum of two decomposed vectors synthesized from two active voltage vectors of that sector ($\vec{V}_{L,1}$ and $\vec{V}_{R,1}$) and two zero-voltage vectors ($\vec{V}_z$) corresponding to the given on-duty times (T_L, T_R, and T_0), respectively.

3. COMPARISON OF DYNAMIC PERFORMANCE IN SIMULATION RESULTS

3.1. Simulation specifications

In this section, there are the evaluation and analysis being conducted by simulation using the MATLAB/ Simulink to assess the dynamic performance between CVC and FVC methods based on simulation outcomes. It implies a comparison between different scenarios of speed and load conditions to determine their dynamic behavior.

The comparison of dynamic characteristics between the two technical control methods above requires ensuring that they are evaluated under identical operating conditions, including speed reference and load values, motor parameters (as given in Table 1), speed controller gains, etc. Additionally, both simulations should be configured with the same sampling step and simulation time to facilitate a meaningful comparison.

Table 1. Specification of target SPMSM

Specification	Value	Unit
DC voltage, V_{dc}	200	V_{DC}
Rated current, i_{rated}	10	A_{pk}
Maximum current, i_{max}	31	A_{pk}
Base speed, N_{base}	3000	rpm
Rated torque, $T_{e,rated}$	3.5	N.m
Pole-pairs, p_n	5	-
Stator resistance, R_s	244.4	mΩ
Permanent magnet flux linkage, Ψ_m	57.3	mWb
Stator inductance, L_s	1.81	mH

3.2. Speed and Torque performance comparative results

In this section, the comparative analysis of speed and torque performance between the CVC and FVC schemes as presented in Fig. 5 offers valuable insights into their efficacy in motor control. This assessment encompasses the examination of diverse performance metrics, including speed response, torque response (evaluating torque ripple and transient torque response), and steady-state performance.

Fig. 6 provides a closer look at transient states, specifically regions 1 and 2, as depicted in Fig. 5. This zoomed-in view allows for a more detailed examination of the dynamics during these specific time intervals, offering insights into the behavior of the control system under transient conditions. These observations are supported by the response time data observed during speed-up regions (from 0.0s to 0.5s) in Fig. 6(a) and under sudden loading conditions of the motor (at t = 1.0s) in Fig. 6(b).

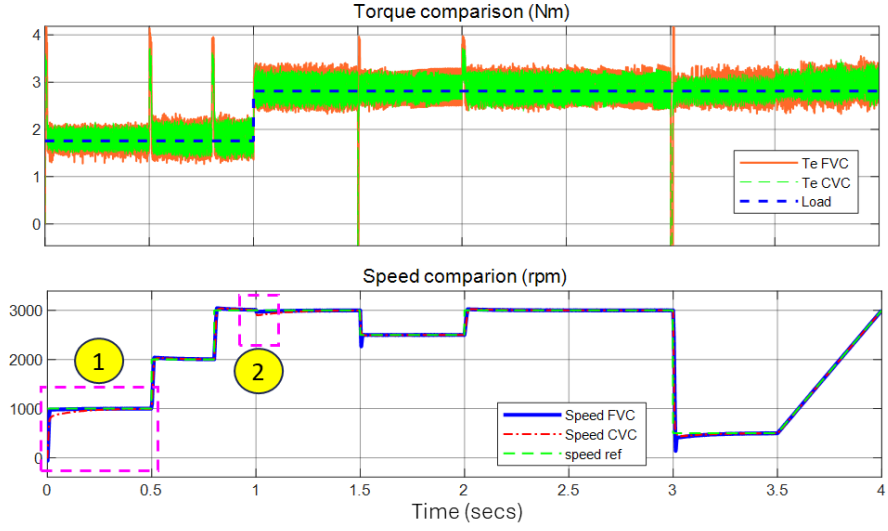

Figure 5. The comparative results of speed and torque performance between the CVC and FVC schemes

As depicted in Fig. 6(a), the response time for speed is recorded as 0.02s for the FVC scheme, which is faster compared to 0.04s for the CVC scheme.

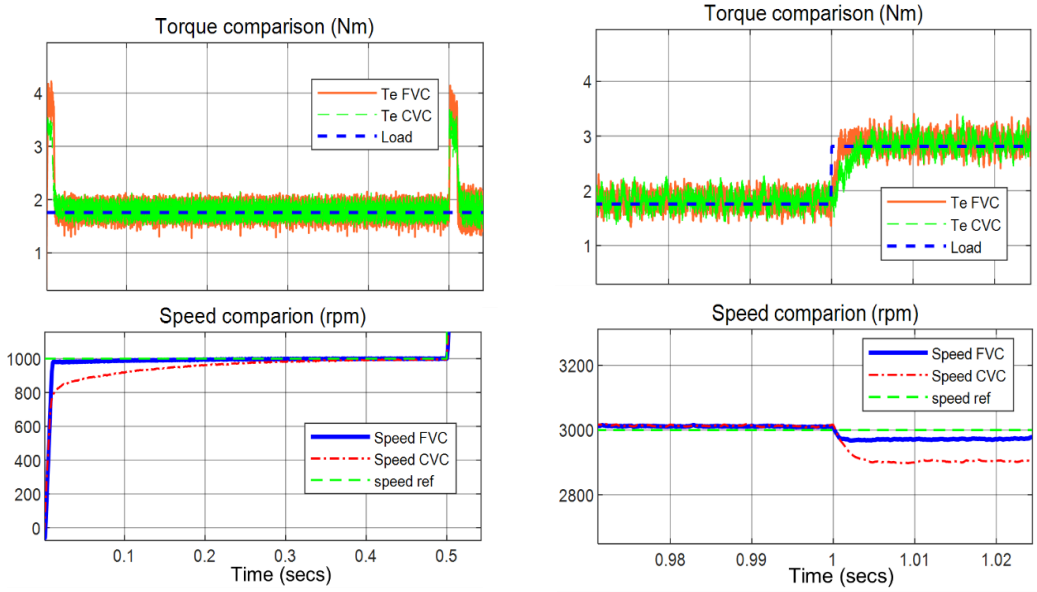

(a) Zoom-in region 1 *(b)* Zoom-in region 2

Figure 6. Zoom-in at two regions (1 and 2) indicated in Fig. 5

As seen in Fig. 6(b), upon sudden application of load to the motor, a decrease in speed of approximately 100 rpm is observed for the CVC scheme, whereas for the FVC scheme, the decrease is around 30 rpm. Additionally, the actual torque curve in the FVC scheme tracks slightly better compared to that in the CVC scheme.

Terms of the torque response, both methods exhibit consistent performance across various load and speed conditions, as depicted in Fig. 5. However, upon closer examination of the transient state, it is observed that the FVC scheme yields slightly higher torque compared to the CVC scheme. Additionally, the torque ripple of the FVC scheme is slightly greater than that of the CVC scheme in steady-state conditions, as indicated in Fig. 6. Moreover, during transient loading states, the torque response of the FVC scheme demonstrates greater robustness compared to that of the CVC scheme, as illustrated in Fig. 6(b).

3.3. Current waveform comparative results

To evaluate the impact of control strategies on motor current distortion, FFT analysis results of the current waveform for phase A at steady-state under heavy load and high speed are conducted, as depicted in Fig. 7 and 8.

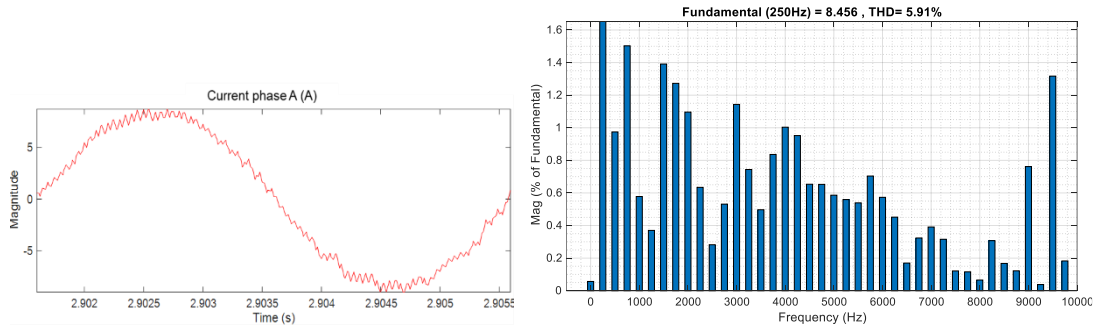

(a) Current waveform of phase A at t = 2.9s *(b)* FFT analysis of current phase A at t = 2.9s

Figure 7. Performing FFT analysis of the current phase A at steady-state for the CVC scheme under the full load and base speed condition

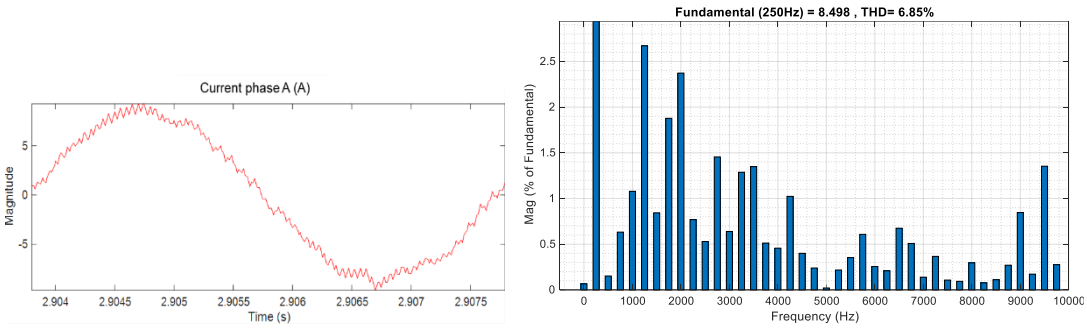

(a) Current waveform of phase A at t = 2.9s *(b)* FFT analysis of current phase A at t = 2.9s

Figure 8. Performing FFT analysis of the current phase A at steady-state for the FVC scheme under the full load and base speed condition

While both methods exhibit similar trends in current values at steady-state, as presented in Fig.s 7(a) and 8(a), there are notable differences in the shape of the current waveforms during operation. Based on the analysis of Total Harmonic Distortion (THD) in the steady-state currents of phase A for both methods, it is evident that the THD of the current waveform in the FVC scheme is 6.58% larger compared to that of the CVC scheme (5.91%), as illustrated in Fig.s 7(b) and 8(b).

4. CONCLUSION

This work has compared control methods for SPMSM drives based on the Current Vector and Flux Vector. It can be found that both methods possess distinct advantages, with the FVC method offering simplicity in control scheme, while the CVC method provides precise and smooth current regulation.

The simulation analysis conducted in this study has revealed that the FVC scheme demonstrates a faster response speed during acceleration and less speed drop when subjected to sudden heavy loads, representing better kinematic performance compared to CVC. Although both methods exhibit similar dynamic responses under various load and speed conditions, there are slight differences observed in torque ripple (less ripple in the CVC scheme) and transient torque response (slightly stronger dynamic in the FVC scheme). In steady-state conditions, the current waveform in the CVC scheme exhibits less distortion compared to that in the FVC scheme.

Overall, the findings of this study provide valuable insights for engineers and researchers in selecting the most appropriate control strategy for PMSM drives, with the choice between them dependent on specific application requirements.

REFERENCES

1. Noguchi T. - Trends of permanent-magnet synchronous machine drives. IEEJ Transactions on Electrical and Electronic Engineering **2** (2) (2007) 125-142. https://doi.org/10.1002/tee.20119
2. Matsuoka K. - Development trend of the permanent magnet synchronous motor for railway traction. IEEJ Transactions on Electrical and Electronic Engineering **2** (2) (2007) 154-161. https://doi.org/10.1002/tee.20119

3. Mishra P. A. A., Srivastava S. - A comprehensive analysis and implementation of vector control of permanent magnet synchronous motor. International Journal of Power Energy Conversion (2014). https://doi.org/10.1504/IJPEC.2014.059982
4. Casadei D., Profumo F., Serra G., Tani A. - FOC and DTC: Two viable schemes for induction motors torque control. IEEE Transactions on Power Electronics **17** (5) (2002) 779-787. https://doi.org/10.1109/Tpel.2002.802183
5. Tang L., Zhong L., Rahman M. F., Hu Y. - A novel direct torque controlled interior permanent magnet synchronous machine drive with low ripple in flux and torque and fixed switching frequency. IEEE Transactions on Power Electronics **19** (2) (2004) 346-354. https://doi.org/10.1109/TPEL.2003.823170
6. Ton, T.-D., Hsieh, M.-F. - A deadbeat current and flux vector control for IPMSM drive with high dynamic performance. Applied Sciences **12** (2022) 3789. https://doi.org/10.3390/app12083789
7. Sun T., Wang J., Jia C., Peng L. - Integration of FOC with DFVC for interior permanent magnet synchronous machine drives. IEEE Access **8** (2020) 97935-97945. https://doi.org/10.1109/ACCESS.2020.2996948
8. Buja G., Kazmierkowski M. - Direct torque control of PWM inverter-fed AC motors - a survey. IEEE Transactions on Industrial Electronics **51** (4) (2004) 744–757. https://doi.org/10.1109/TIE.2004.831717
9. Jo G. J., Choi J. W. - Gopinath model-based voltage model flux observer design for field-oriented control of induction motor. IEEE Transactions on Power Electronics 34 (5) (2019) 4581-4592. https://doi.org/10.1109/Tpel.2018.2864322

TÓM TẮT

NGHIÊN CỨU SO SÁNH CHIẾN LƯỢC ĐIỀU KHIỂN VÉC TƠ DÒNG ĐIỆN VÀ VÉC TƠ TỪ THÔNG CHO ĐỘNG CƠ ĐỒNG BỘ NAM CHÂM VĨNH CỬU

Tôn Thất Đồng[1]*, Nguyễn Khánh Quang[2], Nguyễn Đăng Khoa[3]
[1]*Trường Cao đẳng Công nghiệp Huế*
[2]*Trường Đại học Bách Khoa - Đại học Đà Nẵng*
[3]*Công ty Cổ phần SYSBOTIX Solution*
*Email: *ttdong@hueic.edu.vn*

Nghiên cứu này so sánh hiệu quả điều khiển giữa phương pháp điều khiển véc tơ dòng điện (CVC) và véc tơ từ thông (FVC) cho hệ truyền động điện động cơ đồng bộ nam châm vĩnh cửu cực lồi (SPMSM). Chiến lược điều khiển của hai phương pháp trên được trình bày và phân tích trong nghiên cứu này. Thông qua kết quả mô phỏng, hiệu suất truyền động tạo ra bởi động cơ tương ứng với hai phương pháp điều khiển được đánh giá và so sánh cả trong trạng thái biến đổi nhất thời và trạng thái xác lập. Kết quả thu được từ nghiên cứu phân tích này có thể hỗ trợ các kỹ sư trong việc lựa chọn chiến lược điều khiển phù hợp nhất cho các ứng dụng sử dụng động cơ PMSM.

Từ khóa: Điều khiển véc tơ dòng điện, điều khiển véc tơ từ thông, động cơ đồng bộ nam châm vĩnh cửu, điều khiển tựa từ trường (FOC).